Bioorg. Med. Chem. 72 (2022) 116945

Contents lists available at ScienceDirect

Bioorganic & Medicinal Chemistry

journal homepage: www.elsevier.com/locate/bmc

Polyguluronate simulations shed light onto the therapeutic action of OligoG CF-5/20

Oliver J. Hills [a,*], Chin W. Yong [b,c], Andrew J. Scott [d], James Smith [a], Helen F. Chappell [a,*]

[a] School of Food Science & Nutrition, University of Leeds, Woodhouse Lane, Leeds LS2 9JT, UK
[b] Scientific Computing Department, Science and Technology Facilities Council, Daresbury Laboratory, Keckwick Lane, Daresbury, Warrington, WA4 4AD, UK
[c] Division of Pharmacy and Optometry, School of Health Sciences, University of Manchester, Oxford Road, Manchester M13 9PL, UK
[d] School of Chemical & Process Engineering, University of Leeds, Woodhouse Lane, Leeds LS2 9JT, UK

ARTICLE INFO

Keywords:
P. aeruginosa
OligoG CF-5/20
Density-functional theory
Molecular dynamics
Mucoid biofilms

ABSTRACT

Chronic mucoid *P. aeruginosa* cystic fibrosis (CF) lung infections are associated with the development of a biofilm composed of anionic acetylated exopolysaccharide (EPS) alginate, electrostatically stabilised by extracellular Ca^{2+} ions. OligoG CF-5/20, a low molecular weight guluronate rich oligomer, is emerging as a novel therapeutic capable of disrupting mature *P. aeruginosa* biofilms. However, its method of therapeutic action on the mucoid biofilm EPS is not definitively known at a molecular level. This work, utilising molecular dynamics (MD) and Density-Functional Theory (DFT), has revealed that OligoG CF-5/20 interaction with the EPS is facilitated solely through bridging Ca^{2+} ions, which are not liberated from their native EPS binding sites upon OligoG CF-5/20 dispersal, suggesting that OligoG CF-5/20 does not cause disruptions to mature *P. aeruginosa* biofilms through breaking EPS-Ca^{2+}-EPS ionic cross-links. Rather it is likely that the therapeutic activity arises from sequestering free Ca^{2+} ions and preventing further Ca^{2+} induced EPS aggregation.

1. Introduction

Cystic Fibrosis (CF) is a recessively inherited, life-threatening disease. The pathophysiological cascade in CF patients begins with the Cystic Fibrosis Transmembrane Conductance Regulator (CFTR) gene defect. This reduces the quality and quantity of the CFTR protein, leading to defective ion transport, airway-surface liquid depletion and, subsequently, reduced mucociliary clearance,[1] creating a prime infection site for *Pseudomonas aeruginosa*. Quantitative microbiological analysis of CF sputum from live CF patients has highlighted incidences of *P. aeruginosa* infections reaching 89 %, occurring far more frequently than other common bacterial infections, implicating *P. aeruginosa* as the most clinically problematic pathogen in CF sufferers.[2] Upon colonisation of the CF lung, transcriptional activation of the alginate biosynthetic gene cluster (*algD*) drives the conversion to the mucoid phenotype.[3] The pathogenicity and chronicity of this phenotype is attributed to its ability to form an anionic acetylated exopolysaccharide (EPS) alginate-rich biofilm[4] that is cross-linked by a number of ions that are found in elevated concentrations in CF sputum (Ca^{2+}, Mg^{2+}, Fe^{3+} and Na^{+} [5]). This cross-linking forms densely aggregated, electrostatically stabilized cross-linked matrices that are mechanically stable[6–7] and resistant to pharmacological challenge.[8] Recent Density-Functional Theory (DFT) based molecular modelling highlighted calcium ions as potent ionic cross-linkers, with the capacity to out-compete other sputum ions for EPS binding, giving rise to thermodynamically stable cross-linked EPS scaffolds. This emphasizes the role of calcium in biofilm chronicity.[9]

Upon biofilm establishment in the CF lung, the movement of quorum sensing autoinducer (QSAI) molecules between bacterial subpopulations coordinates virulence, further biofilm matrix proliferation and the maintenance of biofilm matrix architecture.[10–11] An illustration of a mucoid *P. aeruginosa* biofilm matrix is given in Fig 1, detailing *P. aeruginosa* colonies enveloped within calcium cross-linked EPS material, which constitutes the primary scaffold of the mucoid biofilm matrix in the CF lung.

OligoG CF-5/20 is a low molecular weight, guluronate rich (>85 % guluronate) oligomer that is able to disrupt mature mucoid *P. aeruginosa* biofilm matrices[12] and, as such, is considered as the basis of emerging novel anti-Pseudomonal agents. Previous testing showed that exposing mature mucoid *P. aeruginosa* biofilms to 5 % OligoG resulted in a 2.5 log reduction in bacterial CFU as well as potentiated the antimicrobial effects of the antibiotic colistin, highlighting the potential synergy that can be achieved through OligoG-antimicrobial combined therapies.[13]

* Corresponding authors.
E-mail addresses: fsojh@leeds.ac.uk, H.F.Chappell@leeds.ac.uk (H.F. Chappell).

https://doi.org/10.1016/j.bmc.2022.116945
Received 30 May 2022; Received in revised form 19 July 2022; Accepted 21 July 2022
Available online 26 July 2022

OligoG CF-5/20 is an anionic oligomer under physiological conditions, possessing negatively charged carboxylate groups that facilitate irreversible binding to the bacterial cell surface, in turn increasing the net negative charge of the cell surface and inhibiting bacterial motility and aggregation.[14] These observations, namely, the OligoG CF-5/20 *membrane effects*, have been further corroborated through scanning electron microscopy (SEM) and confocal laser scanning microscopy (CLSM) experiments, which show that the oligomer is able to damage the bacterial cell membrane, potentially, by displacing Ca^{2+} and/or Mg^{2+} ions.[15] Significantly, membrane destruction, through the loss of stabilising Ca^{2+} and/or Mg^{2+} ions, does not lead to adaptive OligoG CF-5/20 resistance after prolonged exposure.[15] In fact, *P. aeruginosa* cultivated in the presence of OligoG CF-5/20 has fewer colonies with multi-drug resistant (MDR) phenotypes and improved antibiotic susceptibilities.[16]

A recent combined SEM and molecular dynamics (MD) study on eDNA, another *P. aeruginosa* matrix component, showed that the OligoG CF-5/20 carboxylate groups can chelate Ca^{2+}, preventing Ca^{2+}-induced ionic cross-linking.[12] What results, as can be observed through atomic force microscopy (AFM), SEM and CLSM, are *P. aeruginosa* biofilm matrices that are irregular and less compact,[15,17] with a reduced Young's modulus.[17] Given that calcium exposure is a large contributor to the increase in the Young's modulus of mucoid *P. aeruginosa* biofilms,[18] calcium chelation chemistry is very likely underlying the observed matrix disruption effects of OligoG CF-5/20. By extension, OligoG CF-5/20 therapy is able to normalise CF mucus by outcompeting mucin (MUC2N) for the binding of Ca^{2+} ions, meaning MUC2N will remain unfolded and easier to clear.[19] Although the global matrix disruption effects of OligoG CF-5/20 have been observed *in vitro* and *in vivo*, hypothetical OligoG CF-5/20 disruption mechanisms at an atomistic level have only been tested against eDNA structures.[12] The disruption effect on the mucoid EPS scaffold has not been explored and, as such, is unknown at an atomistic level, despite it being the major component of mucoid *P. aeruginosa* CF biofilms.[4,20]

To this end, the aim of this study was to investigate the modes of interaction between OligoG CF-5/20 and the mucoid *P. aeruginosa* EPS, as well as quantify the thermodynamic stability of the EPS-OligoG CF-5/20 adducts, using a combined MD-DFT theoretical molecular modelling approach. This approach allows an exploration of modes of interaction exhibited by OligoG CF-5/20 as well as pinpointing functionality vital for forming thermodynamically stable interactions with the EPS. A molecular model of a thermodynamically stable Ca^{2+} cross-linked acetylated copolymeric β-D-mannuronate-α-L-guluronate 2-chain system was previously developed within the group.[9] Its step-wise development, accommodation of structural motifs unique to mucoid *P. aeruginosa* and validation against available *in vivo* and *ex vivo* experimental data has been previously provided.[9] This model has since been further developed into a thermally equilibrated hydrated 4-chain model, which has a geometry more representative of the structure at physiological equilibrium, and possesses a discontinuous, dendritic, V-shaped morphology.[21] This particular morphology matches the *in vitro* morphology observed in transmission electron microscopy (TEM) and amphiphilic carbon quantum dot visualisations of the mucoid *P. aeruginosa* biofilms.[22,23] This multi-chain model of calcium-complexed EPS, is ideally suited to study interactions with OligoG CF-5/20.

OligoG CF-5/20 is therapeutically active at a range of different polymer lengths.[19] Here, in this work, a guluronate quadramer (Poly-α-L-guluronate quadramer; Poly-G_4) was chosen as a model to represent OligoG CF-5/20 and this structure can be seen in **Figure S1.** Poly-G_4 possesses the correct guluronate abundance, is on a 1:1 length scale with the EPS molecular model, and allows for tractability when calculating the thermodynamic stabilities from DFT. The Poly-G_4 molecule was thermally equilibrated at physiological temperature in explicit water to obtain a representative *in vivo* conformation, and then combined with the EPS structure for subsequent MD simulations (see **Materials & methods**).

2. Materials & methods

All molecular dynamics trajectories were computed using DL_POLY_4.[24] The conversion of all molecular models into DL_POLY input files was performed using DL_FIELD.[25] Trajectories were computed with the OPLS2005 forcefield[26,27] in the canonical (NVT) ensemble. The RATTLE algorithm[28] was used to constrain covalent bonds to hydrogen, meaning the integration time-step could be increased to 2 ps. The temperature was held at 310 K (body temperature) using Langevin thermostatting[29]. Electrostatics were treated using the Smooth-Particle-Mesh-Ewald method[30] and the distance cut-offs for electrostatic and Leonard-Jones interactions were set to 1.2 nm.

Poly-G_4 was thermally equilibrated at 310 K in Simple Point Charge (SPC) water, under periodic boundary conditions, in a simulation cell measuring 40 Å × 40 Å × 40 Å over 1 ns. The thermally equilibrated

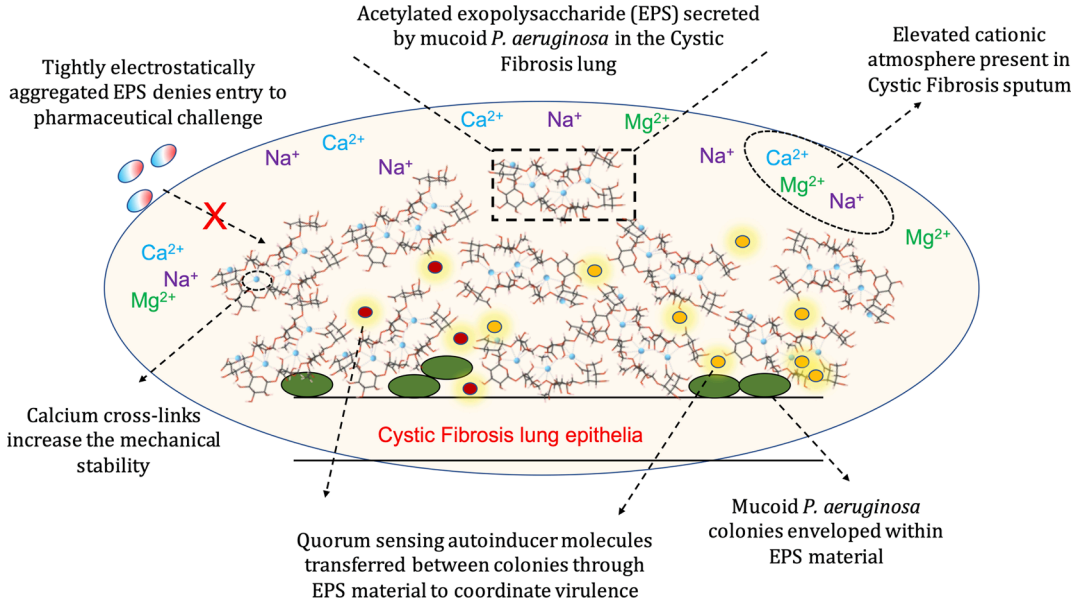

Fig. 1. A general illustration of a mucoid *P. aeruginosa* biofilm matrix established within the Cystic Fibrosis (CF) lung.

Poly-G_4 (Figure S1) encompasses a torsional profile in good agreement with the torsional profile predicted for the ground state conformation of acidic β-1–4 linked guluronate disaccharides (ϕ = -82°, ψ=-155°), obtained from the MM3 forcefield (a forcefield that, along-side OPLS2005, can accurately reproduce the geometries of biomacromolecules and small organic molecules[31]) based molecular mechanics minimisations, in the work of Braccini *et al.*[32] The thermally equilibrated Poly-G_4 molecule was positioned 6 Å away from the base of the V-shaped cleft in the EPS structure, a suitable distance to ensure no significant hydrophobic or electrostatic interactions between the Poly-G_4 and the EPS. Subsequent EPS-Poly-G_4 simulations were performed in SPC water, under periodic boundary conditions, in a simulation cell measuring 60 Å × 60 Å × 60 Å, over 10 ns. This trajectory length is sufficient to allow the Poly-G_4 system to sample preferential binding sites and adopt an equilibrium binding configuration with the EPS.

All Density Functional Theory (DFT) calculations were performed using the plane-wave Density Functional Theory (DFT) code, CASTEP.[33] A convergence tested cut-off energy of 900 eV was employed, as well as a Monkhorst-Pack *k*-point grid of 1 × 1 × 1 to sample the Brillouin zone.[34] On-the-fly ultrasoft pseudopotentials were used[35] alongside the PBE exchange–correlation functional[36] coupled with the semi-empirical dispersion correction scheme of Tkatchenko and Scheffler,[37] to account for intra- and intermolecular dispersive forces. 0 K *in vacuo* DFT single-point energy calculations were performed using an SCF tolerance set to 2×10^{-6} eV Atom^{-1}. Mulliken bond populations[38] were calculated to classify the nature of bonding between the EPS and the Poly-G_4 in each of the final EPS-Poly-G_4 adducts. The thermodynamic stability of the isolated EPS-Poly-G_4 adducts were evaluated by means of a formation energy (**Equation (1)**).

$$E_f = E_{\{EPS-Poly-G_4 adduct\}} - \left(E_{\{EPS\}} + E_{\{Poly-G_4\}}\right) \quad (1)$$

where $E_{\{EPS-Poly-G_4 adduct\}}$ is the energy of the EPS-Poly-G_4 adduct, $E_{\{EPS\}}$ is the energy of the EPS molecular model and $E_{\{Poly-G_4\}}$ is the energy of the thermally equilibrated Poly-G_4 molecule (Fig S1).

3. Results and discussion

Bound EPS–Poly-G_4 adducts displayed at 2 ns intervals, and their formation energies (according to **Equation (1)**) are shown in Fig 2.

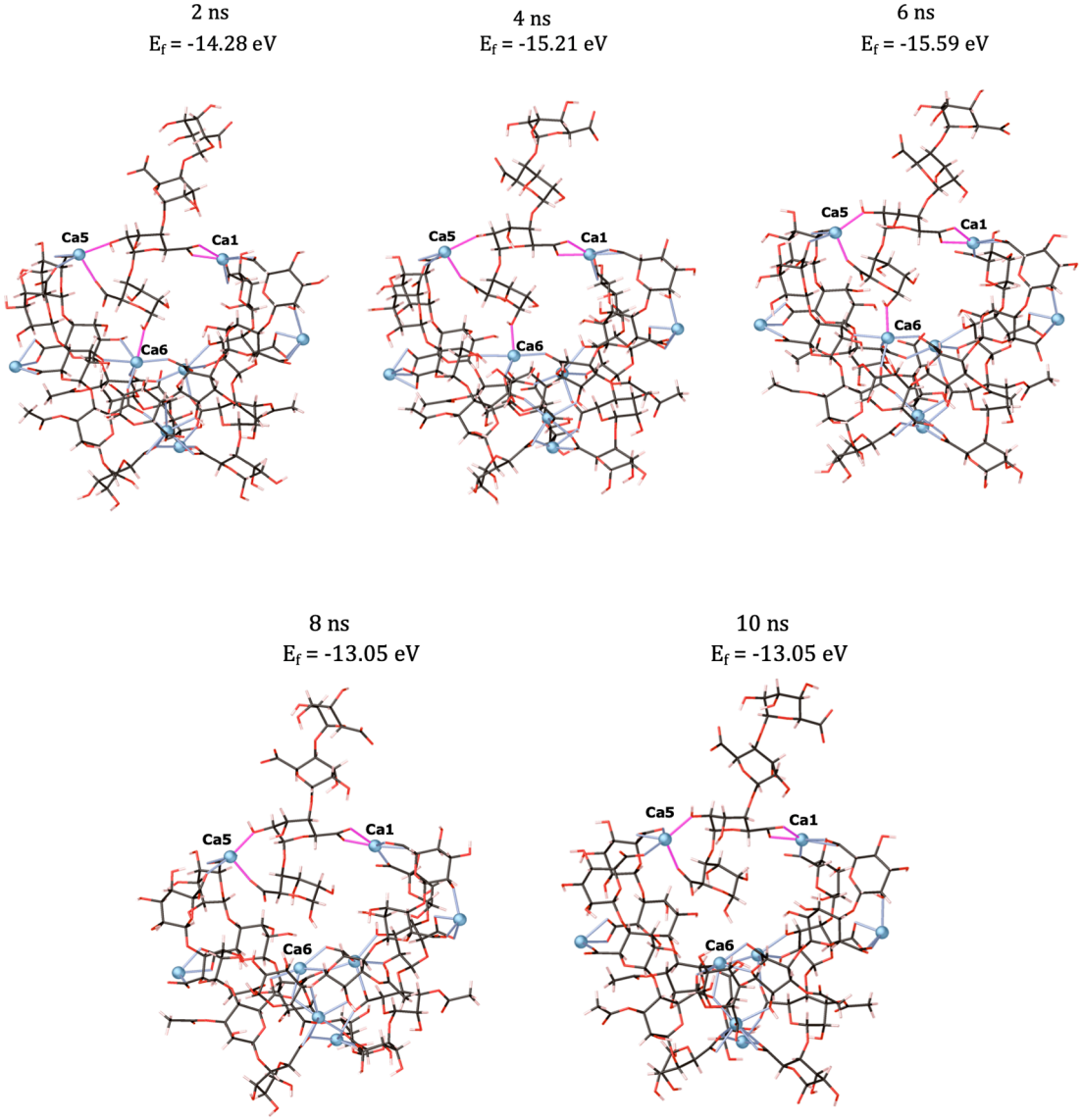

Fig. 2. Bound EPS-Poly-G_4 adducts, along with their formation energies, displayed every 2 ns. Carbon atoms are shown in grey, oxygen in red, calcium in blue and hydrogen in pink. Calcium-oxygen ionic bonds are shown with blue lines and calcium ions implicated in binding of Poly-G_4 are labelled. Ionic bonds between the Poly-G_4 and the EPS system are shown with bold pink lines.

The Poly-G_4 system binds in a thermodynamically stable fashion, returning a negative formation energy for each adduct within the V-shaped cleft (Fig 2). On binding, the adducts establish ionic bonds to the EPS-bound Ca^{2+} ions through carboxylate and hydroxyl functional groups. Previous MD simulations, studying the interactions between OligoG CF-5/20 and respiratory mucin, have also implicated the hydroxyl group(s) in binding.[39] Specifically, hydrogen bonding interactions were observed between the guluronate hydroxyl groups and nitrogen and/or oxygen atoms on the mucin peptide backbone.[39] However, the Poly-G_4 molecule in our simulations does not show any hydrogen bonding interaction with the EPS chains and all interactions are facilitated by bridging Ca^{2+} ions. Indeed, Ca^{2+} ions being the main facilitator of OligoG CF-5/20 interactions with host molecular systems has also been observed in FTIR measurements on eDNA - OligoG CF-5/20,[12] as well as in small angle neutron scattering and circular dichroism measurements on lipopolysaccharide (LPS) - OligoG CF-5/20.[40]

The Poly-G_4 system adopts a bound configuration which is stable over time and remains bound throughout its entire trajectory (10 ns). The oligomer does not liberate the cleft and experiences only minor conformational changes ($\leq 5°$) to its uronate backbone, indicating that ionic association to the Ca^{2+} ions in the EPS significantly reduces the molecule's mobility and flexibility. Essentially, upon binding to EPS-bound Ca^{2+} ions, the Poly-G_4 system is rendered irreversibly bound and immobile. This can be exemplified by considering the RMSD, as well as the torsional change about the G3-G4 junction (**Figure S1**), between the 2 ns and 10 ns bound structures. Explicitly, the EPS-Poly-G_4 2–10 ns RMSD is 1.18 Å and, interestingly, considering the Poly-G_4 backbone in isolation of the EPS, the 2–10 ns RMSD is also 1.18 Å. The change in ϕ and ψ angles across the G3-G4 junction, where the ionic O-Ca^{2+} tethers are established, are 5° and 4° respectively over the same time period. For reference, the RMSD between the pre-equilibrated and post-equilibrated Poly-G_4 structures is 4.24 Å, with maximum torsional changes in ϕ and ψ angles of 43° and 44° respectively. This, evidently, illustrates that the highly energetically favourable bound Poly-G_4 configuration, adopted early in the trajectory (2 ns), is resistant to further conformational change over the remainder of the 10 ns trajectory.

Displayed in Tables 1 and 2 (and illustrated graphically in **Fig S2**) are the average COO^--Ca^{2+} and HO-Ca^{2+} Mulliken populations (|e|) and lengths (Å) for the EPS-Poly-G_4 tethering contacts displayed at 2 ns intervals. These tables highlight the sustained stability of the EPS-Poly-G_4 tethering contacts over the time course of the trajectory.

Within each structure, it is clear to see that all O-Ca^{2+} tethers are ionic in nature, possessing Mulliken populations $\leq$ 0.12 |e|. Furthermore, the COO^--Ca^{2+} tethers are the most stable tethering contact within each structure, as indicated by their shorter average lengths and larger average Mulliken populations. In fact, considering all COO^--Ca^{2+} and HO-Ca^{2+} tethers, averaged over the full course of the 10 ns trajectory, the carboxylate tethers are 0.17 Å shorter (2.25 Å) compared to the hydroxyl tethers (2.42 Å). The mode of COO^--Ca^{2+} binding remains constant over the course of the trajectory, specifically, the monodentate COO^--Ca5 and bidentate COO^--Ca1 binding modes remain in place over the full 10 ns (Fig. 2). In addition, both the HO-Ca^{2+} and COO^--Ca^{2+} tethers retain consistency in their lengths and Mulliken populations, with their respective averages fluctuating within one standard deviation over the 10 ns trajectory (**Fig S2**). Taken collectively it is clear that, upon Poly-G_4 binding, established hydroxyl and carboxyl tethers retain their stability over 10 ns. The only exception to this is the hydroxyl contact, HO-Ca6, which is present throughout the first 6 ns, but afterwards is lost and not present in the final structure at the end of the trajectory. Between 6 and 8 ns, Ca6 sinks deeper into the V-shaped cleft, losing its interaction with the invading Poly-G_4 OH group (Fig. 3). This results in a 1.63 Å increase in the HO-Ca6 distance, positioning the Ca6 out of the hydroxyl ionic bonding range. The effective "sinking" of Ca6 can be rationalised by considering the EPS V-angle, namely, the Ca5-Ca6-Ca1 angle (Fig. 2**)** that defines the V-shaped motif. These measurements are given in Table 3.

Table 1
Average EPS- Poly-G_4 O-Ca^{2+} Mulliken populations (|e|) calculated at 2 ns intervals. Note, from 8 ns only a single Poly-G_4 HO-Ca^{2+} interaction exists.

Time (ns)	Average COO-Ca population (|e|)	(±) std	Average OH-Ca population (|e|)	(±) std
2	0.11	0.045	0.075	0.005
4	0.10	0.050	0.085	0.015
6	0.11	0.059	0.085	0.005
8	0.12	0.057	0.060	–
10	0.11	0.057	0.075	–

Table 2
Average EPS- Poly-G_4 O-Ca^{2+} lengths (Å) calculated at 2 ns intervals. Note, from 8 ns only a single Poly-G_4 HO-Ca^{2+} interaction exists.

Time (ns)	Average COO-Ca length (Å)	(±) std	Average OH-Ca length (Å)	(±) std
2	2.29	0.014	2.42	0.060
4	2.23	0.044	2.52	0.061
6	2.23	0.044	2.38	0.047
8	2.26	0.083	2.37	–
10	2.29	0.083	2.42	–

Before 6 ns, the EPS V-angle fluctuates between 66°- 69°. But after 6 ns, there is a contraction in the V-angle to 60°, lowering Ca6 deeper into the cleft and away from the invading Poly-G_4 OH group. The HO-Ca5 interaction does survive the full time-scale of the trajectory, however, it only does so because Ca5 is held in its position through the invading monodentate COO^--Ca5 interaction. This suggests that the hydroxyl tethering contacts are not primarily responsible for keeping OligoG CF-5/20 bound to the mucoid *P. aeruginosa* biofilm EPS. Rather, it is the COO^- group, more so than the OH group, that facilitates the primary molecular mechanism of action, leading to the therapeutic effects such as "antibiotic synergy" and "quorum sensing antagonism",[13,41] which are observed over long time-scales.

The EPS-Poly-G_4 configurations adopted at 8 ns and 10 ns possess identical formation energies (-13.05 eV), EPS V-angle and Poly-G_4 binding geometry, the latter of which captures the site-directed calcium chelation modes observed both experimentally and theoretically when OligoG CF-5/20 is dispersed within CF airway mucin,[19,39] eDNA[12] and *P. aeruginosa* EPS scaffolds.[42] This is a strong indicator that the Poly-G_4 system has adopted an equilibrium binding configuration within 10 ns. This is in agreement with the time-scales required to identify an equilibrium binding geometry between OligoG CF-5/20 and CF airway mucin detailed in previous MD simulations.[39] Additionally, the minor deviation in RMSD (1.18 Å) between the 2 and 10 ns states indicates, potentially, that the Poly-G_4 molecule adopts a binding configuration already very close to equilibrium within 2 ns. In fact, low energy, conformationally static, equilibrium calcium binding configurations adopted upon complexation with a single polyguluronate chain have been shown to occur within time-scales as low as 0.8 ns[43,44] and 6 ns[45,46] for 10-mer and 30-mer uronate length scales respectively.

In light of the above, it can be inferred that the Poly-G_4 system would be reluctant to undergo further conformational change in the vicinity of the EPS post 10 ns. Interestingly, the adducts at 8 ns and 10 ns are less thermodynamically stable than the adducts that occur at 2 ns, 4 ns and 6 ns. It is clear, therefore, that although HO-Ca6 is an ionic interaction that does not survive the full time-scale of the trajectory, it is an interaction that assists in stabilising the overall EPS-Poly-G_4 complex. As such, it is interesting to note that although hydroxyl functional groups are not modulators of irreversible binding, they are modulators of overall complex stability. The participation of the hydroxyl group in binding biofilm Ca^{2+} ions was absent in previous MD simulations of combined OligoG CF-5/20 – eDNA structures over 50 ns,[12] and therefore, these simulations highlight for the first time the role of the hydroxyl group in mediating exothermic penetration into the EPS scaffold. The contraction of the EPS V-angle effectively encapsulates the invading

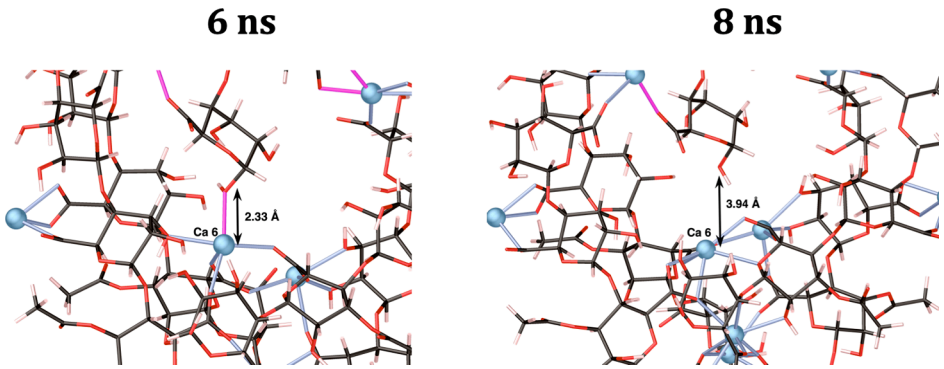

Fig. 3. A close up of the bound EPS-Poly-G_4 adducts at 6 and 8 ns, highlighting the depression of Ca6 into the EPS cleft. Carbon atoms are shown in grey, oxygen in red, calcium in blue and hydrogen in pink. Calcium-oxygen ionic bonds are shown with blue lines and ionic bonds between the Poly-G_4 and EPS system are shown with bold pink lines.

Table 3
The EPS V-angle, namely, the angle formed between Ca5-Ca6-Ca1, which defines the EPS V-shaped motif, calculated at 2 ns intervals.

Time (ns)	EPS V-angle (°)
2	66
4	69
6	68
8	60
10	60

Poly-G_4 molecule and repositions Ca6 out of the Poly-G_4 OH ionic bonding distance. As a consequence, it is anticipated that this particular EPS conformational change nullifies the kinetic behaviour of the OH-Ca^{2+} interaction, specifically preventing the re-establishment of this tethering contact post 10 ns.

To test whether the immobility of the Poly-G_4 system, upon EPS binding, was due to its size (as it is on a 1:1 length scale with the EPS), the Poly-G_4 system was halved to a dimer; Poly-G_2. The system was thermally equilibrated under the same conditions and combined with the EPS in the same fashion as the Poly-G_4 system (see **Materials & methods**). The EPS-Poly-G_2 adducts, displayed at 2 ns intervals, are given in Fig 4 along with their formation energies which were calculated according to **Equation (1)** where $E_{\{Poly-G_4\}}$ is replaced with $E_{\{Poly-G_2\}}$.

Similar to the Poly-G_4 system, the Poly-G_2 dimer is able to bind

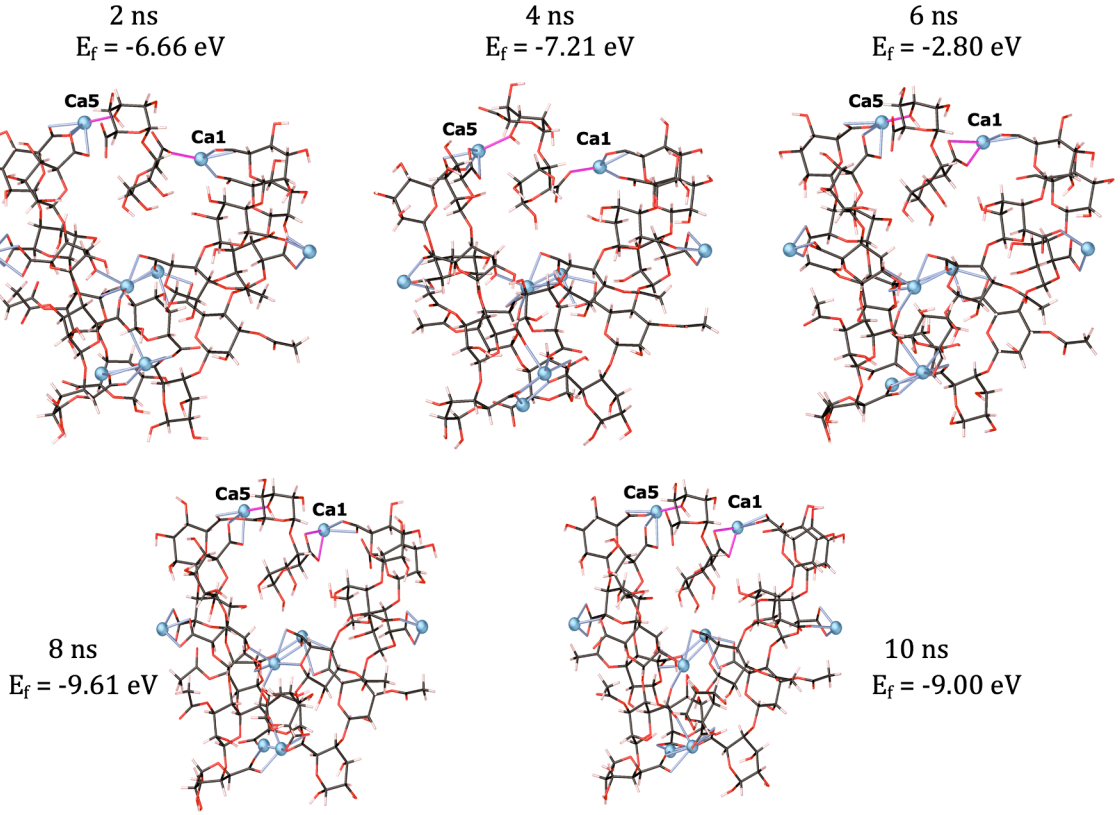

Fig. 4. Bound EPS-Poly-G_2 adducts, along with their formation energies, displayed every 2 ns. Carbon atoms are shown in grey, oxygen in red, calcium in blue and hydrogen in pink. Calcium-oxygen ionic bonds are shown with blue lines and calcium ions implicated in binding of Poly-G_2 are labelled. Ionic bonds between the Poly-G_2 and the EPS system are shown with bold pink lines.

within the V-shaped cleft through hydroxyl and carboxylate ionic tethering contacts to Ca^{2+} ions. Again, no hydrogen bonding interactions are observed between the invading Poly-G_2 and the EPS, and all interactions are facilitated through the EPS Ca^{2+} ions only. The smaller size of the Poly-G_2 does not lead to any increased mobility compared to the Poly-G_4 system and the dimer remains bound to the EPS within the cleft for the full 10 ns. The thermodynamic stabilities, as defined by the formation energies, are approximately half those of the EPS-Poly-G_4 systems, which is intriguing, as it would suggest that matching the polyguluronate and EPS length scales results in more exothermic penetration. The only inconsistency in the trend in EPS-Poly-G_2 adduct stabilities is the structure present at 6 ns. The reason for the gain in instability at this time-step is because Ca1 is undergoing a transition from the monodentate EPS carboxylate O24 site to settle in the more stable bidentate Poly-G_2 carboxylate O12 + O13 binding site (**Fig S3**). This newly established bidentate carboxylate binding mode to Ca1 is stable over the remainder of the 10 ns trajectory. Although illustrating how EPS Ca^{2+} ions can transition between COO^- binding sites, it also shows that the Ca^{2+} ion (Ca1) is still retained in a chelate complex with the EPS and is not liberated from the EPS chains.

Ca5 and Ca1 ions are implicated in facilitating the interaction(s) of both the Poly-G_4 and Poly-G_2 systems with the EPS scaffold. Given this circumstance, Ca5 and Ca1 were removed from the EPS-Poly-G_2 starting structure, and the MD simulation repeated for another 10 ns, to gauge the response of the Poly-G_2 dimer, and to see if it would be encouraged to liberate the V-shaped cleft. The EPS-Poly-G_2 adduct occurring at 10 ns in this trajectory can be seen in Fig 5.

The Poly-G_2 sinks deeper into the cleft, reorienting to position a single COO^- group to face Ca6 and Ca2 and, in turn, establishing three ionic tethering contacts to these ions, in preference to liberating the cleft of the EPS scaffold. Only ionic interactions are present in this structure and, thus, the cationic charge density present in the EPS, despite the removal of Ca5 and Ca1, is still sufficient to retain the Poly-G_2 dimer in the EPS vicinity and subsequently bind electrostatically. This, therefore, further highlights the authority Ca^{2+} ions have in mediating interactions between polyguluronate structures and the EPS chains.

The EPS-Poly-G_4 simulations, alongside the EPS-Poly-G_2 simulations, highlight that the Ca^{2+} ions are not liberated from the EPS chains by the invading OligoG CF-5/20. Specifically, native EPS bound Ca^{2+} ions retain their chelate geometries bound to EPS oxygen functionality upon OligoG CF-5/20 invasion – these ions are not pulled away from the EPS chains and the invading OligoG CF-5/20 causes no disruption to the EPS ionic scaffold. Over the full time-scale of the Poly-G_4 trajectory, the orientation of the EPS carboxylate groups remains unchanged - continuously facing the Ca^{2+} ions. Circular dichroism measurements on systems of OligoG CF-5/20 dispersed in *P. aeruginosa* biofilms, also observe no change in bacterial alginate carboxylate orientation.[42] Alongside this, the overall V-shaped morphology of the model is maintained throughout the full time-scale of the trajectory, meaning the Poly-G_4 system does not force a complete separation of the 4-chain EPS structure into two sets of 2-chains or any other smaller units. The definition of the V-angle was introduced above, and the measurements are displayed in Table 3. The EPS V-angle decreases from 69° to 60° over the 10 ns, showing that, in fact, the EPS chains become closer together as opposed to further apart upon Poly-G_4 binding, encapsulating the invading Poly-G_4. As such, the invasion of Poly-G_4 does not rupture the original ionic architecture present within the EPS scaffolds through displacing Ca^{2+} or destroying ionic cross-links.

In light of these observations above, the proposed mechanism of disruption, when mucoid *P. aeruginosa* biofilm matrices are exposed to OligoG CF-5/20, involves a non-disruptive invasion of the Ca^{2+} cross-links. This stimulates Poly-G_4 encapsulation which, in turn, prevents

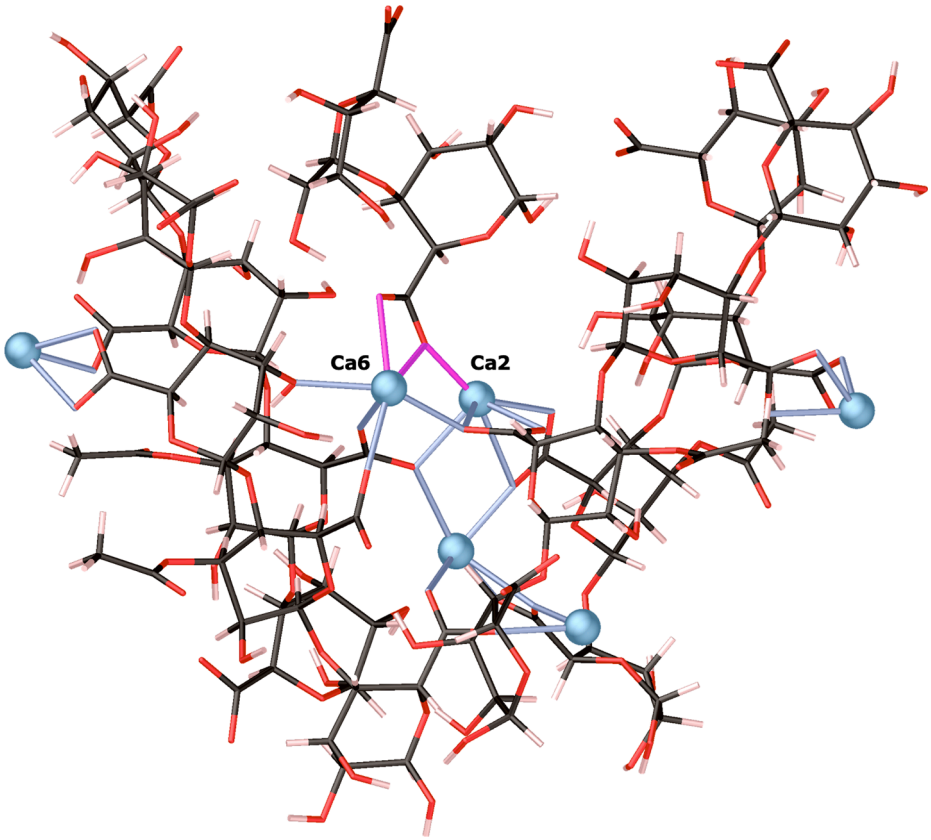

Fig. 5. The EPS-Poly-G_2 adduct at 10 ns following removal of Ca1 and Ca5 from the starting structure. Carbon atoms are shown in grey, oxygen in red, calcium in blue and hydrogen in pink. Calcium-oxygen ionic bonds are shown with blue lines and ionic bonds between the Poly-G_2 and the EPS system are shown with bold pink lines.

both the sequestration of free (unbound) Ca^{2+} ions by the EPS, as well as, further Ca^{2+} mediated EPS aggregation. This mode of action draws significant comparisons with the proposed mode of action of eDNA exposed to OligoG CF-5/20, which was also elucidated through previous MD simulations.[12]

4. Conclusion

OligoG CF-5/20 is an exciting, novel anti-Pseudomonas therapeutic targeted at treating chronic mucoid *P. aeruginosa* biofilm infections in the CF lung. The OligoG CF-5/20 induced global matrix disruption effects, although having been observed *in vitro* and *in vivo* on bulk living biofilms, are currently unknown mechanistically at an atomistic level. To shed light onto the matrix disruption mechanism, a large-scale Ca^{2+} cross-linked EPS molecular model, representing the primary mucoid *P. aeruginosa* CF lung biofilm matrix component with the correct ionic composition, has been combined with a guluronate quadramer and dimer (Poly-G_4 and Poly-G_2 molecular models of the OligoG CF-5/20 system) in a combined MD-DFT theoretical approach.

These simulations have captured the coordination chemistry responsible for driving exothermic dispersal of OligoG CF-5/20 into the EPS. Specifically, these simulations have identified that carboxylate and hydroxyl functional groups are responsible for establishing thermodynamically stable EPS-Poly-G_4 and Poly-G_2 adducts, although the former is most likely responsible for irreversible binding and, as such, the therapeutic effects which are observed over long time-scales. Furthermore, these simulations have highlighted that Ca^{2+} ions are critically important in mediating the interactions between OligoG CF-5/20 and the EPS chains with only electrostatic interactions driving the binding events. Although Ca^{2+} behaves as an OligoG CF-5/20 *binding facilitator*, these ions are not liberated from the EPS chains and the effectively benign effects on the EPS ionic architecture posed by the invading OligoG CF-5/20 allow the EPS to retain its V-shaped conformation, with no EPS chain separation being observed.

Simulations of the Poly-G_2 dimer led to thermodynamically stable EPS adducts, showing large similarities in binding modality to the Poly-G_4 system. The removal of key Ca^{2+} ions, which acted as tethering points for the invading guluronate, did not lead to an absence of Poly-G_2 binding as the dimer was able to sink deeper into the discontinuous cleft in the EPS architecture and reorient a carboxylate group to sustain new ionic O-Ca^{2+} interactions. The greater thermodynamic stability of the EPS-Poly-G_4 adducts, relative to the Poly-G_2 adducts, would suggest that OligoG CF-5/20 molecules on a similar length scale to the EPS chains are capable of more exothermic EPS dispersal. The similarities between the Poly-G_4 and Poly-G_2 simulations suggest that it is Ca^{2+} ion affinity that keeps the guluronate molecule tethered to the EPS, rather than its size, and further highlights that the EPS bound Ca^{2+} ions give impetus to OligoG CF-5/20 dispersal.

Overall, the matrix disruption mechanism posed by OligoG CF-5/20 involves EPS encapsulation, which prevents the sequestration of free (unbound) Ca^{2+} ions by the EPS, as well as preventing further Ca^{2+} mediated EPS aggregation.

Data Availability Statement:

All data generated or analysed during this study are included in this published article (and its Supplementary Information files).

CRediT authorship contribution statement

Oliver J. Hills: Conceptualization, Methodology, Investigation, Visualization, Writing – original draft, Writing – review & editing. **Chin W. Yong:** Methodology, Writing – review & editing. **Andrew J. Scott:** Supervision, Writing – review & editing. **James Smith:** Supervision, Writing – review & editing. **Helen F. Chappell:** Supervision, Writing – original draft, Writing – review & editing.

Declaration of Competing Interest

The authors declare that they have no known competing financial interests or personal relationships that could have appeared to influence the work reported in this paper.

Data availability

All data generated or analysed during this study are included in this published article (and its Supplementary Information files).

Acknowledgements

This work was undertaken on ARC4, part of the High-Performance Computing facilities at the University of Leeds, UK. CY was supported by CoSeC, the Computational Science Centre for Research Communities, which was made available through the Material Chemistry Consortium.

Funding

The author(s) received no specific funding for this work.

Appendix A. Supplementary data

Supplementary data to this article can be found online at https://doi.org/10.1016/j.bmc.2022.116945.

References

1 Lubamba B, Dhooghe B, Noel S, Leal T. Cystic fibrosis: insight into CFTR pathophysiology and pharmacotherapy. *Clin Biochem*. 2012;45:1132–1144.
2 Bauernfeind A, Hörl G, Jungwirth R, et al. Qualitative and quantitative microbiological analysis of sputa of 102 patients with cystic fibrosis. *Infection*. 1987;15:270–277.
3 Chitnis CE, Ohman DE. Genetic analysis of the alginate biosynthetic gene cluster of *Pseudomonas aeruginosa* shows evidence of an operonic structure. *Mol Microbiol*. 1993;8:583–590.
4 Evans LR, Linker A. Production and characterization of the slime polysaccharide of *Pseudomonas aeruginosa*. *J Bacteriol*. 1973;116:915–924.
5 Smith DJ, Anderson GJ, Bell SC, Reid DW. Elevated metal concentrations in the CF airway correlate with cellular injury and disease severity. *J Cyst Fibros*. 2014;13:289–295.
6 Wloka M, Rehage H, Flemming H, Wingender J. Rheological properties of viscoelastic biofilm extracellular polymeric substances and comparison to the behavior of calcium alginate gels. *Colloid Polym Sci*. 2004;282:1067–1076.
7 Wloka M, Rehage H, Flemming H, Wingender J. Structure and rheological behaviour of the extracellular polymeric substance network of mucoid Pseudomonas aeruginosa biofilms. *Biofilms*. 2005;2:275–283.
8 Koo H, Allan RN, Howlin RP, Stoodley P, Hall-Stoodley L. Targeting microbial biofilms: current and prospective therapeutic strategies. Nat Rev Microbiol [Internet]. 2017;15(12):740–55. Available from: https://doi.org/10.1038/nrmicro.2017.99.
9 Hills OJ, Smith J, Scott AJ, Devine DA, Chappell HF. Cation complexation by mucoid Pseudomonas aeruginosa extracellular polysaccharide. Deshpande PA, editor. PLoS One [Internet]. 2021 Sep 2 [cited 2021 Sep 6];16(9):e0257026. Available from: https://journals.plos.org/plosone/article?id=10.1371/journal.pone.0257026.
10 Alayande AB, Aung MM, Kim IS. Correlation Between Quorum Sensing Signal Molecules and *Pseudomonas aeruginosa's* Biofilm Development and Virulency. Curr Microbiol [Internet]. 2018 Feb 9 [cited 2021 Oct 21];75(7):787–93. Available from: https://link.springer.com/article/10.1007/s00284-018-1449-5.
11 Favre-Bonté S, Köhler T, Van Delden C. Biofilm formation by *Pseudomonas aeruginosa*: role of the C4-HSL cell-to-cell signal and inhibition by azithromycin. J Antimicrob Chemother [Internet]. 2003 Oct 1 [cited 2021 Oct 21];52(4):598–604. Available from: https://academic.oup.com/jac/article/52/4/598/713730.
12 Powell LC, Pritchard MF, Ferguson EL, Powell KA, Patel SU, Rye PD, et al. Targeted disruption of the extracellular polymeric network of *Pseudomonas aeruginosa* biofilms by alginate oligosaccharides. NPJ biofilms microbiomes [Internet]. 2018 Dec 29 [cited 2019 Aug 7];4(1):13. Available from: http://www.nature.com/articles/s41522-018-0056-3.
13 Hengzhuang W, Song Z, Ciofu O, Onsøyen E, Rye PD, Høiby N. OligoG CF-5/20 disruption of mucoid *Pseudomonas aeruginosa* biofilm in a murine lung infection model. Antimicrob Agents Chemother [Internet]. 2016 May 1 [cited 2021 Apr 19];60(5):2620–6. Available from: http://aac.asm.org/.
14 Powell LC, Pritchard MF, Emanuel C, Onsøyen E, Rye PD, Wright CJ, et al. A nanoscale characterization of the interaction of a novel alginate oligomer with the cell surface and motility of *Pseudomonas aeruginosa*. Am J Respir Cell Mol Biol

[Internet]. 2014 Mar 3 [cited 2021 Apr 19];50(3):483–92. Available from: http://www.atsjournals.org/doi/abs/10.1165/rcmb.2013-0287OC.
15 Khan S, Tøndervik A, Sletta H, et al. Overcoming drug resistance with alginate oligosaccharides able to potentiate the action of selected antibiotics. *Antimicrob Agents Chemother [Internet].*. 2012. Oct [cited 2021 Nov 17];56(10):5134. Available from: /pmc/articles/PMC3457396/.
16 Oakley JL, Weiser R, Powell LC, Forton J, Mahenthiralingam E, Rye PD, et al. Phenotypic and Genotypic Adaptations in *Pseudomonas aeruginosa* Biofilms following Long-Term Exposure to an Alginate Oligomer Therapy. mSphere [Internet]. 2021 Jan 20 [cited 2021 Apr 19];6(1). Available from: www.ClinicalTrials.gov.
17 Powell LC, Sowedan A, Khan S, Wright CJ, Hawkins K, Onsøyen E, et al. The effect of alginate oligosaccharides on the mechanical properties of Gram-negative biofilms. Biofouling [Internet]. 2013 Apr [cited 2021 Apr 19];29(4):413–21. Available from: http://www.tandfonline.com/doi/abs/10.1080/08927014.2013.777954.
18 Körstgens V, Flemming H, Wingender J, Borchard W. Influence of calcium ions on the mechanical properties of a model biofilm of mucoid Pseudomonas aeruginosa. *Water Sci Technol.* 2001;43:49–57.
19 Ermund A, Recktenwald CV, Skjåk-Braek G, et al. OligoG CF-5/20 normalizes cystic fibrosis mucus by chelating calcium. *Clin Exp Pharmacol Physiol [Internet].* 2017;44:639–647. https://doi.org/10.1111/1440-1681.12744. Available from: Jun 1 [cited 2021 Apr 12.
20 Linker A, Jones RS. A New Polysaccharide Resembling Alginic Acid Isolated from *Pseudomonads*. J Biol Chem [Internet]. 1966 [cited 2020 May 21];241(16):3845–51. Available from: http://www.jbc.org/.
21 Hills OJ, Yong CW, Scott AJ, Devine DA, Smith J, Chappell HF. Atomic-scale interactions between quorum sensing autoinducer molecules and the mucoid *P. aeruginosa* exopolysaccharide matrix. Sci Rep [Internet]. 2022;12(1):7724. Available from: https://doi.org/10.1038/s41598-022-11499-9.
22 Hunter RC, Beveridge TJ. High-resolution visualization of *Pseudomonas aeruginosa* PAO1 biofilms by freeze-substitution Transmission Electron Microscopy. *J Bacteriol [Internet].*. 2005. Nov [cited 2021 Oct 18];187(22):7619. Available from: /pmc/articles/PMC1280322/.
23 Ritenberg M, Nandi S, Kolusheva S, Dandela R, Meijler MM, Jelinek R. Imaging *Pseudomonas aeruginosa* biofilm extracellular polymer scaffolds with amphiphilic carbon dots. *ACS Chem Biol.* 2016;11:1265–1270.
24 T. Todorov I, William Smith, Kostya Trachenko, T. Dove M. DL_POLY_3: new dimensions in molecular dynamics simulations via massive parallelism. J Mater Chem [Internet]. 2006 May 17 [cited 2021 Oct 13];16(20):1911–8. Available from: https://pubs.rsc.org/en/content/articlehtml/2006/jm/b517931a.
25 Yong CW. Descriptions and Implementations of DL_F Notation: A Natural Chemical Expression System of Atom Types for Molecular Simulations. J Chem Inf Model [Internet]. 2016 Aug 22 [cited 2021 Nov 5];56(8):1405–9. Available from: https://pubs.acs.org/doi/full/10.1021/acs.jcim.6b00323.
26 Jorgensen WL, Maxwell DS, Tirado-Rives J. Development and testing of the OPLS all-atom force field on conformational energetics and properties of organic liquids. J Am Chem Soc [Internet]. 1996 Nov 13 [cited 2021 Feb 26];118(45):11225–36. Available from: https://pubs.acs.org/sharingguidelines.
27 Banks JL, Beard HS, Cao Y, Cho AE, Damm W, Farid R, et al. Integrated Modeling Program, Applied Chemical Theory (IMPACT). J Comput Chem [Internet]. 2005 Dec [cited 2021 Feb 26];26(16):1752–80. Available from: /pmc/articles/PMC2742605/.
28 Andersen HC. Rattle: A "velocity" version of the shake algorithm for molecular dynamics calculations. *J Comput Phys.* 1983;52:24–34.
29 Adelman SA, Doll JD. Generalized Langevin equation approach for atom/solid-surface scattering: General formulation for classical scattering off harmonic solids. J Chem Phys [Internet]. 1976 [cited 2021 Oct 27];64:2375. Available from: https://doi.org/10.1063/1.432526.
30 Essmann U, Perera L, Berkowitz ML, Darden T, Lee H, Pedersen LG. A smooth particle mesh Ewald method. J Chem Phys [Internet]. 1998 Aug 31 [cited 2021 Oct 14];103(19):8577. Available from: https://aip.scitation.org/doi/abs/10.1063/1.470117.
31 Stortz CA, Johnson GP, French AD, Csonka GI. Comparison of different force fields for the study of disaccharides. *Carbohydr Res.* 2009;344:2217–2228.
32 Braccini I, Grasso RP, Pérez S. Conformational and configurational features of acidic polysaccharides and their interactions with calcium ions: A molecular modeling investigation. *Carbohydr Res.* 1999;317:119–130.
33 Clark SJ, Segall MD, Pickard CJ, et al. First principles methods using CASTEP. *Z Krist.* 2005;220:567–570.
34 Monkhorst HJ, Pack JD. Special points for Brillouin-zone integrations. *Phys Rev B.* 1976;13:5188.
35 Vanderbilt D. Soft self-consistent pseudopotentials in a generalized eigenvalue formalism. *Phys Rev B.* 1990;41:7892–7895.
36 Perdew JP, Burke K, Ernzerhof M. Generalized gradient approximation made simple. *Phys Rev Lett.* 1996;77:3865.
37 Tkatchenko A, Scheffler M. Accurate molecular van der Waals interactions from ground-state electron density and free-atom reference data. *Phys Rev Lett.* 2009;102,073005.
38 Mulliken RS. Electronic population analysis on LCAO–MO molecular wave functions. *I. J Chem Phys.* 1955;23:1833–1840.
39 Pritchard MF, Powell LC, Menzies GE, Lewis PD, Hawkins K, Wright C, et al. A New Class of Safe Oligosaccharide Polymer Therapy to Modify the Mucus Barrier of Chronic Respiratory Disease. Mol Pharm [Internet]. 2016 Mar 7 [cited 2021 Apr 12];13(3):863–72. Available from: www.hpcwales.
40 Pritchard MF, Powell LC, Khan S, Griffiths PC, Mansour OT, Schweins R, et al. The antimicrobial effects of the alginate oligomer OligoG CF-5/20 are independent of direct bacterial cell membrane disruption. Sci Rep [Internet]. 2017 Mar 31 [cited 2021 Oct 18];7(1):1–12. Available from: https://www.nature.com/articles/srep44731.
41 Jack AA, Khan S, Powell LC, et al. Alginate oligosaccharide-induced modification of the lasI-lasR and rhlI-rhlR quorum-sensing systems in *Pseudomonas aeruginosa*. *Antimicrob Agents Chemother [Internet].*. 2018 https://doi.org/10.1128/AAC.02318-17. May 1 [cited 2021 Apr 19];62(5). Available from:.
42 Pritchard MF, Powell LC, Jack AA, et al. A low-molecular-weight alginate oligosaccharide disrupts *Pseudomonal* microcolony formation and enhances antibiotic effectiveness. *Antimicrob Agents Chemother [Internet].*. 2017. Sep 1 [cited 2021 Jun 16];61(9). Available from: /pmc/articles/PMC5571347/.
43 Stewart MB, Gray SR, Vasiljevic T, Orbell JD. The role of poly-M and poly-GM sequences in the metal-mediated assembly of alginate gels. *Carbohydr Polym.* 2014;4:486–493.
44 Stewart MB, Gray SR, Vasiljevic T, Orbell JD. Exploring the molecular basis for the metal-mediated assembly of alginate gels. *Carbohydr Polym.* 2014;102:246–253.
45 Li ZJ, Srebnik S, Rojas OJ. Revisiting Cation Complexation and Hydrogen Bonding of Single-Chain Polyguluronate Alginate. Biomacromolecules [Internet]. 2021 Sep 13;22(9):4027–36. Available from: https://doi.org/10.1021/acs.biomac.1c00840.
46 Hecht H, Srebnik S. Structural Characterization of Sodium Alginate and Calcium Alginate. Biomacromolecules [Internet]. 2016 Jun 13 [cited 2021 Apr 29];17(6):2160–7. Available from: https://pubs.acs.org/sharingguidelines.